Received: 25 December 2025 | Revised: 15 January 2026 | Accepted: 16 January 2026

DOI: 10.1002/bkcs.70112

ARTICLE

BKCS BULLETIN OF THE KOREAN CHEMICAL SOCIETY

Metal-dependent adsorption and photothermal-assisted catalysis in heterometallic metal–organic frameworks

Eunho Seo[1] | **Dongwook Kim**[2] | **Jinhee Park**[1]

[1]Department of Physics and Chemistry, Daegu Gyeongbuk Institute of Science and Technology (DGIST), Daegu, Republic of Korea

[2]Center for Catalytic Hydrocarbon Functionalization, Institute for Basic Science (IBS), Daejeon, Republic of Korea

Correspondence
Jinhee Park, Department of Physics and Chemistry, Daegu Gyeongbuk Institute of Science and Technology (DGIST), Daegu 42988, Republic of Korea.
Email: jinhee@dgist.ac.kr

Dongwook Kim, Center for Catalytic Hydrocarbon Functionalization, Institute for Basic Science (IBS), Daejeon 34141, Republic of Korea.
Email: dwkimxtal@ibs.re.kr

Funding information
National Research Foundation of Korea, Grant/Award Numbers: RS 2024-00342127, RS-2025-23822979

Abstract

The modular nature of metal–organic frameworks (MOFs) enables structural and functional tuning through controlled combinations of organic linkers and metal ions. Here, we report an isostructural MOF series, M-DGIST-20, constructed from trinuclear $TiM_2(\mu_3\text{-}O)(COO)_6$ (M^{2+} = Ni^{2+}, Co^{2+}, and Mn^{2+}) clusters and a naphthalenediimide-based ligand. The frameworks feature high porosity (≈85% void volume) and serve as a platform to examine composition–function relationships. Iodine adsorption experiments reveal metal-dependent kinetics, with Ni-DGIST-20 showing the fastest uptake due to stronger M–I_2 interactions and higher structural robustness. Post-synthetic coordination of imidazole at open metal sites further increases the adsorption rate and capacity. In addition, efficient photothermal conversion and accessible metal sites in M-DGIST-20 allow localized heating and Lewis acidic catalysis, accelerating the Knoevenagel condensation and subsequent Michael addition-intramolecular cyclization. This study demonstrates how compositional and post-synthetic tuning can modulate adsorption and catalytic activity of MOFs.

KEYWORDS
adsorption, catalysis, metal–organic frameworks, multivariate MOFs, photothermal conversion

Metal–organic frameworks (MOFs) are crystalline porous materials constructed from metal ions or clusters and organic linkers.[1–3] They have drawn significant attention because of their large surface areas, tunable pore structures, and high crystallinity, making them promising in gas storage, separation, sensing, and catalysis.[4–13] However, many MOFs are constructed from a single type of linker or metal ion, and tuning only one component often provides limited control over the resulting functionality. To overcome this limitation, the multivariate strategy has emerged as an effective approach, incorporating multiple linkers or metal ions within a single framework. This approach offers not only a means of compositional control but also opportunities to investigate how composition influences structures and properties. Various mixed-ligand-based multivariate-MOFs (MTV-MOFs), including MTV-MOF-5,[14] MUF-7,[15] PCN-700,[16] and UMCM-1,[17] have been developed as representative examples of frameworks integrating multiple functionalities.[18–21] These materials have been constructed through diverse approaches such as one-pot synthesis using mixed linkers, topological combination of ligands with different connectivities, and sequential ligand installation. In contrast to the extensive development of mixed-ligand systems, synthesizing mixed-metal-based MTV-MOFs[22–28] is far more challenging; different metal ions often exhibit distinct reactivities and coordination preferences, which makes it difficult to obtain highly crystalline frameworks and often results in different crystallinities across metal ions and even amorphous products. Consequently, understanding how metal ion composition influences the structural and functional properties of MOFs remains a challenge.

In parallel with compositional tuning at the metal nodes, post-synthetic incorporation of functional molecules offers another effective handle to modulate framework properties.[29,30] The installation of Lewis-basic ligands such as pyridine derivatives, triazoles, imidazole analogs, and aliphatic amines at open metal sites (OMSs) further modifies the local coordination environment and strengthens host–guest interactions by introducing new binding or reactive sites.[31–34] These newly generated sites enable additional interaction pathways, including acid–base interactions,

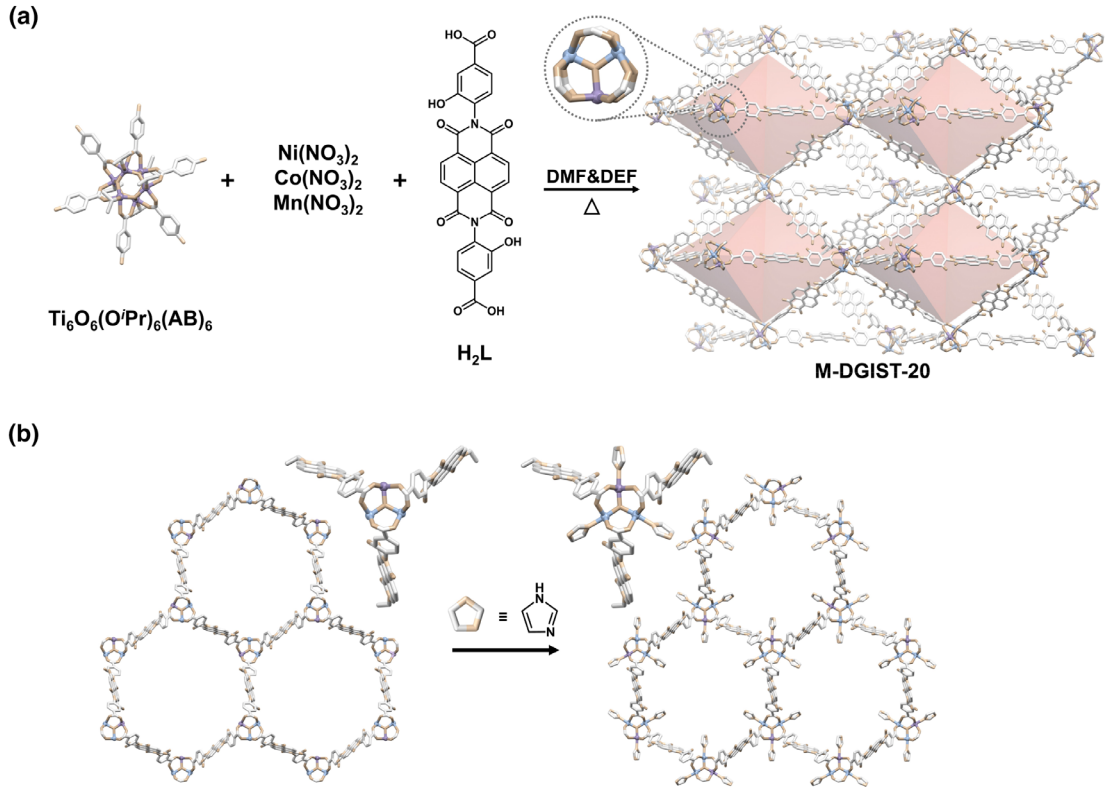

FIGURE 1 (a) Synthetic route of M-DGIST-20 and its single-crystal structure showing the pore architecture and metal node. (b) Structural change of Co-DGIST-20 upon imidazole coordination, yielding IM@Co-DGIST-20.

hydrogen bonding, and σ-/π-donor effects, which in turn facilitate guest inclusion and catalytic activation, thereby extending the functional landscape of MOFs.

In this study, a new series of isostructural MOFs, $TiM_2(\mu_3\text{-}O)L_3$ (M-DGIST-20, M = Ni^{2+}, Co^{2+}, and Mn^{2+}), was synthesized by combining a naphthalenediimide (NDI)-based linker (*N,N*′-bis(3-hydroxybenzoate)-1,4,5,8-naphthalenediimide, L^{2-}) with Ti^{4+} and divalent metal ions. The strong Lewis acidity of Ti^{4+} facilitates the crystallization of isostructural frameworks even in the presence of different M^{2+} ions. Furthermore, the resulting frameworks can incorporate either a single transition-metal ions or multiple ones, yielding mixed-metal MTV MOFs. The M-DGIST-20 series also features a highly open structure with a void volume of approximately 85%. However, the removal of guest solvent molecules induces partial structural collapse due to the combination of large pore volume and the inherent flexibility of the metal nodes.[35,36] Although direct evacuation under vacuum is not feasible, the solvent-containing frameworks retains its structural integrity and provide highly accessible pores and open metal sites (OMSs), offering an excellent platform to systematically investigate how compositional factors, including the incorporated metal ions and post-synthetic coordination of functional molecules, influence overall frameworks behavior.

M-DGIST-20 was solvothermally synthesized by combining H_2L with various Ti^{4+} precursors and M^{2+} nitrates in a 1:1 mixture of *N,N*-dimethylformamide (DMF) and *N,N*-diethylformamide (DEF) at 150 °C. Initially, titanium isopropoxide ($Ti(O^iPr)_4$) and titanium butoxide ($Ti(OBu)_4$) were employed as Ti^{4+} precursors. However, their high reactivity mainly resulted in amorphous products (Figure S7). To address this issue, preformed Ti-oxo clusters were employed to promote more uniform nucleation and crystal growth. Since these clusters contain six-coordinated Ti^{4+} centers, their moderated reactivity allows more controlled crystallization.[37,38] When $Ti_6O_6(O^iPr)_6(t\text{-}BA)_6$ (O^iPr = isopropoxide, *t*-BA = *tert*-butylacetate) was used, the hydrophobic ligands reduced the solubility and overall reactivity, preventing complete reaction and subsequent crystallization. In contrast, $Ti_6O_6(O^iPr)_6(AB)_6$ (AB = 4-aminobenzoate) afforded large and uniform single crystals of Ni-DGIST-20 and Co-DGIST-20 (Figure 2a). These results indicate that the coordination environment around the Ti^{4+} centers critically influences precursor reactivity and that fine-tuning the cluster structure is essential for controlling crystal growth kinetics and improving framework crystallinity.

The crystal structures of Ni- and Co-DGIST-20, determined by single-crystal X-ray diffraction (SCXRD),[39] reveal a three-dimensional network constructed from $TiM_2(\mu_3\text{-}O)(COO)_6$ nodes composed of one Ti^{4+} ion and two divalent transition-metal ions. Within each metal node, all metal ions adopt an octahedral coordination environment, and six L^{2-} ligands are coordinated to each node, with each ligand bridging two adjacent metal nodes. Although

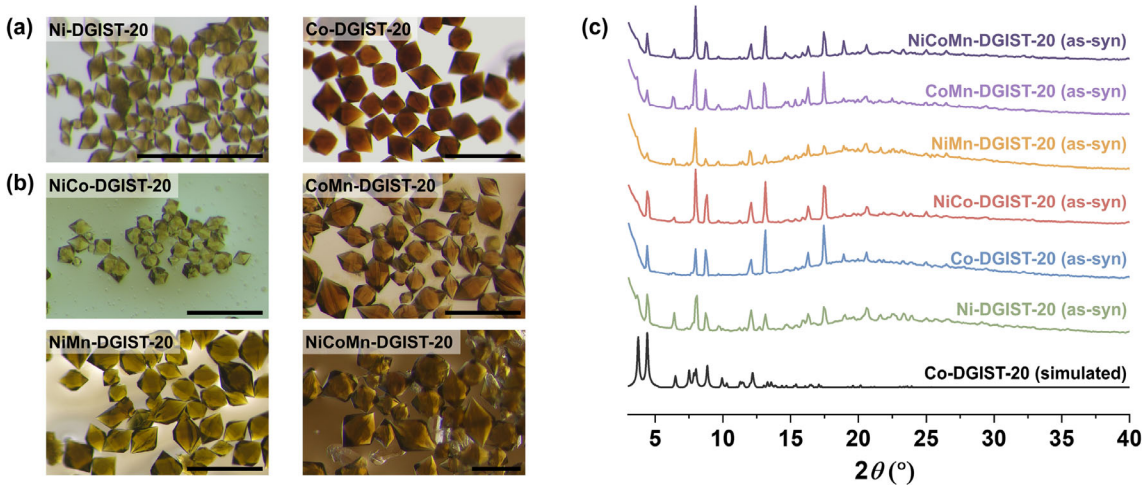

FIGURE 2 Optical microscopy images of M-DGIST-20 incorporating (a) a single and (b) two or three types of transition metal ions (scale bars = 200 μm). (c) PXRD patterns of as-synthesized M-DGIST-20 compared with the simulated pattern of Co-DGIST-20. All the samples were synthesized using benzoic acid as a modulator.

Ni- and Co-DGIST-20 share the same framework topology, their M—O bond lengths differ, with Ni—μ_3-O and Co—μ_3-O distances of 1.958(4) and 2.083(5) Å, respectively. Both frameworks crystallize in the $P6_3/m$ space group and contain trigonal bipyramidal pores (Figure 1a and Table S1).

Furthermore, inspired by our previous study on the mixed-metal MTV-MOF, MM′-DGIST-14,[38] which shares the same metal node as M-DGIST-20 and exhibited enhanced crystallinity, structural stability, and photoactivity upon incorporation of multiple transition metal ions, we attempted the synthesis of M-DGIST-20 using Ti^{4+} ions combined with two or more transition-metal ions (Ni^{2+}, Co^{2+}, and Mn^{2+}) in 1:1:1 or 1:1:1:1 feed ratios. To optimize the crystallization process, various organic and inorganic acids were tested as modulators (Figure S8). Among these, benzoic acid was the most effective, affording not only Ni- and Co-DGIST-20 but also mixed-metal analogs NiCo-, NiMn-, CoMn-, and NiCoMn-DGIST-20 (Figure 2b). Notably, the crystals obtained using benzoic acid exhibited distinct morphologies compared with those synthesized using formic acid; however, their PXRD patterns confirmed that all M-DGIST-20 variants share the same framework structure (Figures 2c and S6). The metal ion compositions and incorporation ratios of each crystal were determined by inductively coupled plasma optical emission spectrometry (ICP-OES) (Table S2), and the co-presence of Ti^{4+} and M^{2+} within individual crystals was verified by scanning electron microscopy-energy dispersive X-ray spectroscopy (SEM-EDS) (Figure S11). Notably, while the synthesis of Mn-DGIST-20 was unsuccessful, Mn^{2+} could be incorporated when combined with Ni^{2+} or Co^{2+}, yielding NiMn-, CoMn-, and NiCoMn-DGIST-20. These results illustrate that multiple metal ions can promote framework formation, suggesting that compositional tuning at the metal nodes offers a promising route to expand structural diversity.

Although M-DGIST-20 possesses a highly open framework structure, the removal of solvent molecules from the pores induces partial structural collapse, resulting in negligible N_2 uptake. Thus, liquid-phase iodine adsorption experiments were conducted to evaluate the accessible porosity and to examine how the incorporated metal ions influence the adsorption behavior. Iodine uptake from cyclohexane was monitored by UV–Vis spectroscopy at exposure times ranging from 1 to 150 h. Among the series, Ni-DGIST-20 exhibited the fastest iodine adsorption kinetics, whereas Co-DGIST-20 was more than two times slower. In contrast, NiCo-DGIST-20, which contains Ni^{2+} and Co^{2+} in an approximately 6:4 ratio, displayed a markedly faster adsorption rate than Co-DGIST-20, underscoring the pronounced kinetic contribution of Ni^{2+}. The adsorption rates followed the order Ni- > NiCo- > Co- ≈ NiCoMn- > NiMn- > CoMn-DGIST-20 (Figure 3a). This trend aligns with the Irving–Williams series ($Ni^{2+} > Co^{2+} > Mn^{2+}$),[40,41] which predicts progressively stronger metal–ligand binding and higher complex stability from Mn^{2+} to Ni^{2+}. Therefore, the stronger coordination environment around Ni^{2+} centers, together with the enhanced structural robustness, appears to be the key factor responsible for the accelerated iodine adsorption observed in Ni-containing MOFs.

Nevertheless, even Ni-DGIST-20, the fastest in the series, exhibited relatively slow adsorption kinetics (96 h to reach 99% removal), indicating that the framework has limited intrinsic affinity toward iodine. Nitrogen-containing moieties such as amine, pyridine, and imidazole are known to interact strongly with iodine.[42–44] Guided by this, M-DGIST-20 crystals were soaked in a 0.1 M imidazole solution, and imidazole was incorporated at the OMSs, as confirmed by SCXRD and ^{1}H NMR analysis (Figures 1b and S3). In Ni-DGIST-20, all OMSs were coordinated within 30 min, whereas in Co-DGIST-20, only about 30% were coordinated in the same period, requiring more than 6 h for complete incorporation due to the weaker binding preference of imidazole for Co^{2+} relative to Ni^{2+} (Figure 3b). The imidazole-modified frameworks, IM@Ni-DGIST-20 and

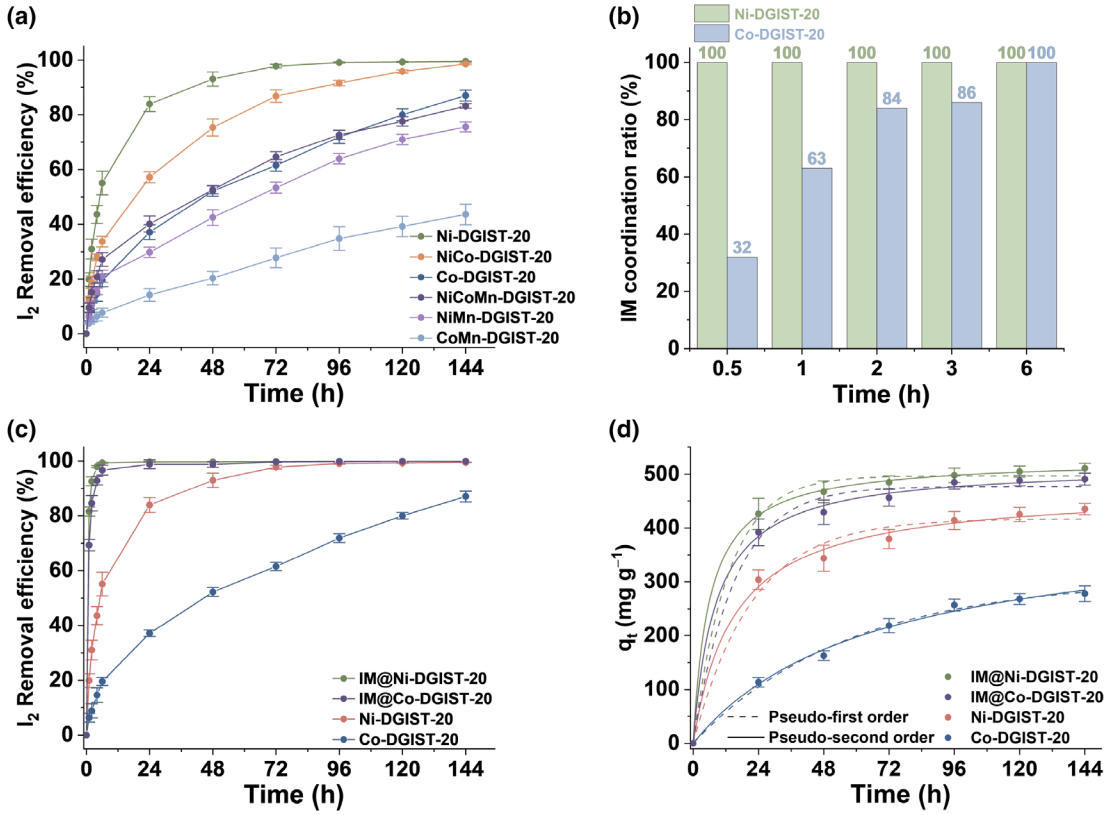

FIGURE 3 (a) Comparison of iodine adsorption kinetics among M-DGIST-20 samples with different metal compositions in 1 mM I_2 solution. (b) Comparison of the imidazole coordination ratio at OMSs of Ni-DGIST-20 and Co-DGIST-20 as a function of treatment time in 0.1 M imidazole solution. Comparison of iodine adsorption kinetics between M-DGIST-20 and IM100@M-DGIST-20 (c) in 1 mM I_2 solution and (d) in 8 mM I_2 solution, fitted using the pseudo-first-order and pseudo-second-order models.

IM@Co-DGIST-20, exhibited significantly enhanced iodine adsorption kinetics. After 4 h of exposure, IM@Ni-DGIST-20 and IM@Co-DGIST-20 achieved iodine removal efficiencies of 98% and 93%, respectively, whereas their pristine counterparts showed only 44% and 15% under the same conditions (Figure 3c). Imidazole coordination also increased the equilibrium iodine uptake. In an 8 mM I_2 solution, pristine Ni-DGIST-20 and Co-DGIST-20 exhibited equilibrium capacities of 473 and 305 mg g^{-1}, respectively, whereas IM@Ni-DGIST-20 and IM@Co-DGIST-20 reached 529 and 518 mg g^{-1}, corresponding to 1.33 and 1.31 I_2 molecules per imidazole (Figure 3d). These results demonstrate that the incorporated imidazole strengthens the interaction between the framework and iodine.

The as-synthesized samples are black crystals due to the formation of $NDI^{\bullet-}$ radicals, generated as formate species act as electron donor during the thermal decomposition of DMF.[45] Upon exposure to air, the crystals rapidly oxidized within 10 min, turning light brown, and this redox process was found to be reversible. Under an inert atmosphere, visible light (405 nm) or IR (808 nm) irradiation in the presence of the electron donor triethylamine restored the dark-colored reduced state (Figure 4a). The formation and disappearance of the $NDI^{\bullet-}$ radicals during these redox cycles were confirmed by EPR analysis (Figure 4b).

The IR responsive redox behavior of M-DGIST-20 motivated further examination of its photothermal properties.[46] The solid-state UV–Vis spectra exhibit weak absorption in the near-infrared region, indicating small energy gaps that favor nonradiative decay pathways (Figure S12). Upon 808 nm irradiation, M-DGIST-20 showed a pronounced temperature rise, reaching 120 °C, whereas the NDI ligand (H_2L) increased only to 80 °C (Figures 4c and S5a). These results confirm that the MOF dissipates absorbed IR energy more effectively as heat.

The photothermal property of M-DGIST-20 enables its use as an internal heat source to drive organic transformations,[47] while the Lewis acidic OMSs function as catalytic sites.[48,49] To evaluate this photothermal-assisted catalytic behavior, M-DGIST-20 was applied to the Knoevenagel condensation of benzaldehyde and malononitrile.[45] In the absence of a catalyst, no product was formed even under external heating at 50 °C (entries 1 and 2 in Table 1). When a suspension containing M-DGIST-20 was irradiated with an 808 nm IR laser for 3 h, the solution temperature increased to approximately 43 °C (Figures 4d and S5b). Under these conditions, Ni-DGIST-20, Co-DGIST-20, and NiCo-DGIST-20 afforded yields of 94%, 94%, and 89%, respectively, which were higher than those obtained under conventional thermal heating at 50 °C (88%, 84%, and 86%, respectively; entries 3–8 in Table 1).

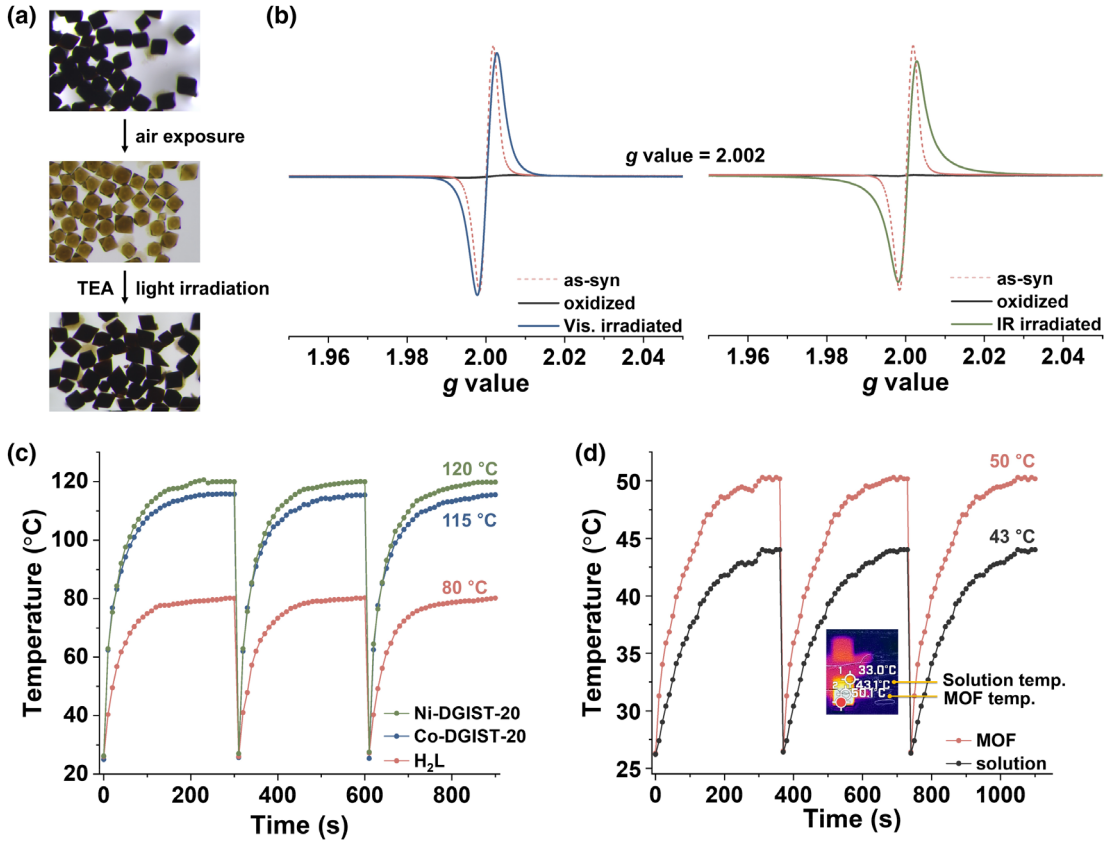

FIGURE 4 (a) Optical microscopy images and (b) corresponding EPR spectra of Ni-DGIST-20 in the as-synthesized, oxidized, and photoinduced reduced states. (c) Repetitive photothermal conversion curves for dried H_2L, Ni-DGIST-20, and Co-DGIST-20. (d) Repetitive photothermal conversion of Ni-DGIST-20 in the Knoevenagel condensation reaction mixture.

TABLE 1 Comparison of catalytic performance in the Knoevenagel condensation of benzaldehyde and malononitrile using 10 mol% catalyst under thermal (50 °C) and IR-induced (808 nm) conditions.

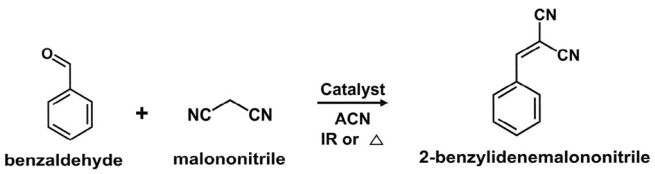

benzaldehyde + malononitrile → 2-benzylidenemalononitrile

Entry	Catalyst/mol%	Reaction condition	Time (h)	Yield (%)
1	No catalyst	ACN, 50 °C	3	0
2	H_2L/10	ACN, 50 °C	3	0
3	Ni-DGIST-20/10	ACN, 50 °C	3	88
4	Ni-DGIST-20/10	ACN, 808 nm	3	**94**
5	Co-DGIST-20/10	ACN, 50 °C	3	84
6	Co-DGIST-20/10	ACN, 808 nm	3	**94**
7	NiCo-DGIST-20/10	ACN, 50 °C	3	86
8	NiCo-DGIST-20/10	ACN, 808 nm	3	**89**
9	Co-DGIST-20/10	ACN, RT	24	24

Note: Yields were determined by ^{1}H NMR. Bold values indicate the yields obtained under IR irradiation, highlighting the superior catalytic performance compared to conventional heating.

A one-pot cascade reaction combining the Knoevenagel condensation and subsequent naphthol integration through Michael addition–intramolecular cyclization was also carried out under the same conditions.[50] Under conventional heating at 50 °C, the yield of 2-amino-4-phenyl-4*H*-benzo[*h*]chromene-3-carbonitrile reached ~80% after 9 h and required 24 h for complete conversion. In contrast, IR irradiation achieved complete conversion within 9 h,

TABLE 2 Comparison of catalytic performance in the Knoevenagel condensation of benzaldehyde and malononitrile and subsequent Michael addition with and without catalysts under thermal (50 °C) and IR-induced (808 nm) conditions.

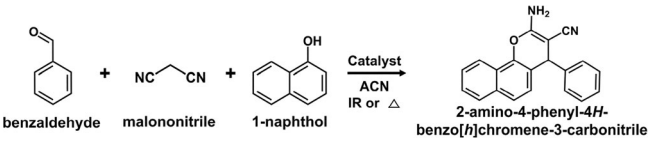

Entry	Catalyst/mol%	Reaction condition	Time (h)	Yield (%)
1	No catalyst/mol%	ACN, 50 °C	9	0
2	H_2L/10	ACN, 50 °C	9	0
3	Ni-DGIST-20/10	ACN, 50 °C	9	82
4	Ni-DGIST-20/10	ACN, 808 nm	9	**100**
5	Co-DGIST-20/10	ACN, 50 °C	9	80
6	Co-DGIST-20/10	ACN, 808 nm	9	**100**
7	NiCo-DGIST-20/10	ACN, 50 °C	9	76
8	NiCo-DGIST-20/10	ACN, 808 nm	9	**99**
9	Co-DGIST-20/10	ACN, RT	24	0

Note: Yields were determined by ^{1}H NMR. Bold values indicate the yields obtained under IR irradiation, highlighting the superior catalytic performance compared to conventional heating.

confirming that the combined catalytic and photothermal functions of M-DGIST-20 substantially enhance the overall reaction rate of this multistep transformation (entries 3–8 in Table 2). These results demonstrate that M-DGIST-20 acts both as a catalyst and as a self-heating medium that accelerates the reaction through localized photothermal heating near the catalytic sites, where transient local temperatures may reach ~120 °C while the bulk solution remains below 50 °C.

CONCLUSION

This study demonstrates that metal-ion compositional control in MOFs serves as an effective strategy to tune their functional behaviors. A new family of heterometallic, isostructural MOFs, M-DGIST-20, was synthesized using an NDI-based linker, Ti^{4+} clusters, and M^{2+} ions (Ni^{2+}, Co^{2+}, Mn^{2+}). Although these materials are nominally porous, which exhibit highly open structures but undergo partial collapse upon activation, their accessible pores under solvated conditions enabled systematic investigation of composition–function relationships. Variation in the incorporated metal ions systematically influenced the iodine adsorption kinetics and framework stability, with Ni-containing structures exhibiting the fastest uptake due to stronger M–I_2 interactions. Furthermore, post-synthetic coordination of imidazole molecules at the OMSs greatly enhanced both the adsorption rate and the overall iodine capacity, underscoring the importance of targeted functionalization in optimizing host–guest interactions. The incorporation of NDI linkers additionally endowed the frameworks with efficient photothermal conversion capability. Combined with the Lewis acidic metal sites, M-DGIST-20 enabled self-heating under IR irradiation and thereby catalyzed thermally driven organic transformations. These findings offer useful guidelines for the rational tuning of MOF compositions toward desired functionalities.

ACKNOWLEDGMENTS

This work was supported by the National Research Foundation (NRF) of Korea, funded by the Ministry of Science and ICT (RS 2024-00342127 and RS-2025-23822979).

FUNDING INFORMATION

National Research Foundation of Korea, Grant/Award Number: RS 2024-00342127 and RS-2025-23822979.

DATA AVAILABILITY STATEMENT

The data that support the findings of this study are available from the corresponding author upon reasonable request.

ORCID

Dongwook Kim https://orcid.org/0000-0003-4432-371X
Jinhee Park https://orcid.org/0000-0001-7755-5889

REFERENCES

[1] H. Furukawa, K. E. Cordova, M. O'Keeffe, O. M. Yaghi, *Science* **2013**, *341*, 1230444.
[2] A. J. Howarth, Y. Liu, P. Li, Z. Li, T. C. Wang, J. T. Hupp, O. K. Farha, *Nat. Rev. Mater.* **2016**, *1*, 15018.
[3] K. Wang, Y. Li, L.-H. Xie, X. Li, J.-R. Li, *Chem. Soc. Rev.* **2022**, *51*, 6417.
[4] O. M. Yaghi, M. O'Keeffe, N. W. Ockwig, H. K. Chae, M. Eddaoudi, J. Kim, *Nature* **2003**, *423*, 705.
[5] C. Wang, D. Liu, W. Lin, *J. Am. Chem. Soc.* **2013**, *135*, 13222.
[6] Y. Wang, H. Lv, E. S. Grape, C. A. Gaggioli, A. Tayal, A. Dharanipragada, T. Willhammar, A. K. Inge, X. Zou, B. Liu, Z. Huang, *J. Am. Chem. Soc.* **2021**, *143*, 6333.
[7] W. Wang, D. Chen, F. Li, X. Xiao, Q. Xu, *Chem* **2024**, *10*, 86.
[8] A. M. Wright, M. T. Kapelewski, S. Marx, O. K. Farha, W. Morris, *Nat. Mater.* **2025**, *24*, 178.

[9] Z.-M. Ye, Y. Xie, K. O. Kirlikovali, S. Xiang, O. K. Farha, B. Chen, *J. Am. Chem. Soc.* **2025**, *147*, 5495.
[10] S. Lee, H. Yoo, J. Y. Kim, *Bull. Korean Chem. Soc.* **2025**, *46*, 918.
[11] G. Gupta, A. Das, C. Y. Lee, *Bull. Korean Chem. Soc.* **2025**, *46*, 1174.
[12] Y. Seo, S. Park, G. Lee, J. Park, H. Oh, E. Lee, *Bull. Korean Chem. Soc.* **2025**, *46*, 1136.
[13] H.-E. Shin, S. H. Yi, D.-W. Lim, *Bull. Korean Chem. Soc.* **2025**, *46*, 1143.
[14] H. Deng, C. J. Doonan, H. Furukawa, R. B. Ferreira, J. Towne, C. B. Knobler, B. Wang, O. M. Yaghi, *Science* **2010**, *327*, 846.
[15] L. Liu, K. Konstas, M. R. Hill, S. G. Telfer, *J. Am. Chem. Soc.* **2013**, *135*, 17731.
[16] S. Yuan, W. Lu, Y.-P. Chen, Q. Zhang, T.-F. Liu, D. Feng, X. Wang, J. Qin, H.-C. Zhou, *J. Am. Chem. Soc.* **2015**, *137*, 3177.
[17] K. Koh, A. G. Wong-Foy, A. J. Matzger, *Angew. Chem. Int. Ed.* **2008**, *47*, 677.
[18] S. Yuan, J.-S. Qin, J. Li, L. Huang, L. Feng, Y. Fang, C. Lollar, J. Pang, L. Zhang, D. Sun, A. Alsalme, T. Cagin, H.-C. Zhou, *Nat. Commun.* **2018**, *9*, 808.
[19] Q. Pang, B. Tu, Q. Li, *Coord. Chem. Rev.* **2019**, *388*, 107.
[20] S. J. Lee, S. G. Telfer, *Angew. Chem. Int. Ed.* **2023**, *62*, e202306341.
[21] W. Jiang, C.-C. Liang, Y.-B. Zhang, *Adv. Funct. Mater.* **2024**, *34*, 2308946.
[22] S. Abednatanzi, P. Gohari Derakhshandeh, H. Depauw, F. X. Coudert, H. Vrielinck, P. Van Der Voort, K. Leus, *Chem. Soc. Rev.* **2019**, *48*, 2535.
[23] M. Y. Masoomi, A. Morsali, A. Dhakshinamoorthy, H. Garcia, *Angew. Chem. Int. Ed.* **2019**, *58*, 15188.
[24] X. Chen, J.-Y. Song, J. Zheng, Y.-M. Wang, J. Luo, P. Weng, B.-C. Cai, X.-C. Lin, G.-H. Ning, D. Li, *J. Am. Chem. Soc.* **2024**, *146*, 19271.
[25] R. E. Sikma, K. S. Butler, D. J. Vogel, J. A. Harvey, D. F. Sava Gallis, *J. Am. Chem. Soc.* **2024**, *146*, 5715.
[26] L. J. Wang, H. Deng, H. Furukawa, F. Gándara, K. E. Cordova, D. Peri, O. M. Yaghi, *Inorg. Chem.* **2014**, *53*, 5881.
[27] W. Xu, H. Chen, K. Jie, Z. Yang, T. Li, S. Dai, *Angew. Chem. Int. Ed.* **2019**, *58*, 5018.
[28] J. Kang, S. Cha, J. Ryu, B. An, C. Lim, Y. Heo, I. Choi, M. Kim, *Bull. Korean Chem. Soc.* **2025**, *46*, 231.
[29] J. D. Evans, C. J. Sumby, C. J. Doonan, *Chem. Soc. Rev.* **2014**, *43*, 5933.
[30] S. M. G. E. Cohen, N. L. G. E. Rosi, *Inorg. Chem.* **2021**, *60*, 11703.
[31] B. Li, Y. Zhang, D. Ma, L. Li, G. Li, G. Li, Z. Shi, S. Feng, *Chem. Commun.* **2012**, *48*, 6151.
[32] J. H. Kim, H. Yun, C. G. Kim, N. Kim, Y. Yang, S. Yoo, D. Moon, D. Kim, C. S. Hong, *J. Am. Chem. Soc.* **2025**, *147*, 37732.
[33] J. H. Choe, H. Kim, H. Yun, J. F. Kurisingal, N. Kim, D. Lee, Y. H. Lee, C. S. Hong, *J. Am. Chem. Soc.* **2024**, *146*, 19337.
[34] J. F. Kurisingal, J. H. Choe, H. Kim, J. Youn, G. Cheon, C. S. Hong, *Bull. Korean Chem. Soc.* **2024**, *45*, 675.
[35] R. Pallach, J. Keupp, K. Terlinden, L. Frentzel-Beyme, M. Kloß, A. Machalica, J. Kotschy, S. K. Vasa, P. A. Chater, C. Sternemann, M. T. Wharmby, R. Linser, R. Schmid, S. Henke, *Nat. Commun.* **2021**, *12*, 4097.
[36] J. R. H. Manning, G. Donval, M. Tolladay, T. L. Underwood, S. C. Parker, T. Düren, *J. Mater. Chem. A* **2023**, *11*, 25929.
[37] Y. Keum, S. Park, Y.-P. Chen, J. Park, *Angew. Chem. Int. Ed.* **2018**, *57*, 14852.
[38] E. Seo, M. Kim, A. Byun, S. Lim, D. Moon, H. Oh, J. Park, *J. Am. Chem. Soc.* **2025**, *147*, 42375.
[39] J. W. Shin, D.-W. Kim, D. Kim, D. Moon, *Bull. Korean Chem. Soc.* **2025**, *46*, 594.
[40] H. Irving, R. J. P. Williams, *J. Chem. Soc.* **1953**, 3192.
[41] H. Irving, R. J. P. Williams, *Nature* **1948**, *162*, 746.
[42] J. T. Hughes, D. F. Sava, T. M. Nenoff, A. Navrotsky, *J. Am. Chem. Soc.* **2013**, *135*, 16256.
[43] L. Liu, N. Wang, C. He, Y. Wei, J. Wang, X. Wang, *J. Hazard. Mater.* **2024**, *480*, 136017.
[44] Z. Wang, Y. Huang, J. Yang, Y. Li, Q. Zhuang, J. Gu, *Dalton Trans.* **2017**, *46*, 7412.
[45] B. Kim, J. Lee, Y.-P. Chen, X.-Q. Wu, J. Kang, H. Jeong, S.-E. Bae, J.-R. Li, J. Sung, J. Park, *Sci. Adv.* **2022**, *8*, eade1383.
[46] Y. Wang, W. Zhu, W. Du, X. Liu, X. Zhang, H. Dong, W. Hu, *Angew. Chem. Int. Ed.* **2018**, *57*, 3963.
[47] J.-D. Xiao, H.-L. Jiang, *Acc. Chem. Res.* **2019**, *52*, 356.
[48] A. Corma, H. García, F. X. Llabrés i Xamena, *Chem. Rev.* **2010**, *110*, 4606.
[49] J. Lee, O. K. Farha, J. Roberts, K. A. Scheidt, S. T. Nguyen, J. T. Hupp, *Chem. Soc. Rev.* **2009**, *38*, 1450.
[50] M. Akbarian, E. Sanchooli, A. R. Oveisi, S. Daliran, *J. Mol. Liq.* **2021**, *325*, 115228.

SUPPORTING INFORMATION

Additional supporting information can be found online in the Supporting Information section at the end of this article.

How to cite this article: E. Seo, D. Kim, J. Park, *Bull. Korean Chem. Soc.* **2026**, *47*(3), 245. https://doi.org/10.1002/bkcs.70112